Charge localization in one-dimensional tetramerized organic conductors: the special case of (tTTF)2ClO4

Arkadiusz Frąckowiak, Roman Świetlik, Olivier Jeannin, Marc Fourmigué, Weiwu Li, Martin Dressel

▶ **To cite this version:**

Arkadiusz Frąckowiak, Roman Świetlik, Olivier Jeannin, Marc Fourmigué, Weiwu Li, et al.. Charge localization in one-dimensional tetramerized organic conductors: the special case of (tTTF)2ClO4 . Journal of Physics: Condensed Matter, 2019, 31 (15), pp.155601. 10.1088/1361-648X/ab00b5 . hal-02015713

HAL Id: hal-02015713

https://univ-rennes.hal.science/hal-02015713

Submitted on 28 Feb 2019

HAL is a multi-disciplinary open access archive for the deposit and dissemination of scientific research documents, whether they are published or not. The documents may come from teaching and research institutions in France or abroad, or from public or private research centers.

L'archive ouverte pluridisciplinaire **HAL**, est destinée au dépôt et à la diffusion de documents scientifiques de niveau recherche, publiés ou non, émanant des établissements d'enseignement et de recherche français ou étrangers, des laboratoires publics ou privés.

Charge localization in one-dimensional tetramerized organic conductors: the special case of $(tTTF)_2ClO_4$

Arkadiusz Frąckowiak[1], Roman Świetlik[1]*, Olivier Jeannin,[2] Marc Fourmigué[2]*, Weiwu Li[3], Martin Dressel[3]

[1] Institute of Molecular Physics, Polish Academy of Sciences,
ul. Mariana Smoluchowskiego 17, 60-179 Poznań, Poland
[2] Univ. Rennes, CNRS, ISCR (Institut des Sciences Chimiques de Rennes)
UMR 6226, 35042 Rennes, France
[3] 1. Physikalisches Institut, Universität Stuttgart, Pfaffenwaldring 57,
70569 Stuttgart, Germany

Corresponding authors:
*Roman Świetlik, e-mail: swietlik@ifmpan.poznan.pl ; tel.: +48 61 8695 165
*Marc Fourmigué: e-mail: marc.fourmigue@univ-rennes1.fr; tel.:+33 (0)2 23 23 52 43

Abstract

We report a detailed structural and spectroscopic study of the one-dimensional 2:1 cation radical salt $(tTTF)_2ClO_4$, where tTTF = trimethylenetetrathiafulvalene, which exhibits a semiconductor-semiconductor phase transition at ca. T = 137 K. Crystal structures are determined above and below the transition; the tTTF molecules in stacks are grouped into weakly interacting tetramers. The reorganization of tTTF stacks is accompanied with an order-disorder transition in anion sublattice. Polarized infrared and Raman spectra of $(tTTF)_2ClO_4$ are measured in the broad frequency range as a function of the temperature (10 - 293 K). The structural and vibrational features are investigated to elucidate the origin of the semiconductor-semiconductor phase transition. We discuss the electron-intramolecular vibration coupling effects in the vibrational spectra of $(tTTF)_2ClO_4$ and identify signatures of high- and low-temperature states of charge localization in the tetramerized system. Both the C=C and C-S stretching modes of tTTF give evidence of strong charge distribution fluctuations in conducting stacks for T >137 K, which are responsible for appearance of molecules with charge +1e , and charge localization in tTTF tetramers for T <137 K. Uniqueness of the salt $(tTTF)_2ClO_4$ in comparison with other tetramerized one-dimensional systems is discussed.

Accepted Manuscript

1. Introduction

In quasi-one-dimensional (1-D) organic cation-radical salts the delocalization of charge carriers in the conducting stacks strongly competes with electron-electron and electron-phonon interactions, which tend to localize the electrons. The subtle interplay between charge, spin, and lattice degrees of freedom is responsible for a rich variety of electronic ground states. Among 1-D conductors formed by tetrathiafulvalene (TTF) derivatives with various counter-ions, the most intensively explored are the salts $(TMTTF)_2X$ and $(TMTSF)_2X$ (X = PF_6, AsF_6, ReO_4, ClO_4, …), in which charge localization, charge ordering, spin-Peierls state, magnetic ordering, spin density waves, and superconductivity are observed [1]. In most 1-D organic conductors the stacks are not uniform but exhibit dimerized, trimerized, tetramerized or even *n*-merized structures. Weakly dimerized structures are responsible for the existence of an energy gap, seen in the activated charge transport or optical absorption. Consequently, despite the 2:1 stoichiometry, in dimerized systems the electronic band is effectively half-filled. On the other hand, strictly uniform conducting stacks with a quarter-filled band (in terms of holes) were also discovered in several 2:1 charge-transfer salts, particularly when they were based on asymmetrical TTF derivatives, such as *o*-DMTTF [2, 3, 4, 5], DMtTTF [6, 7, 8, 9, 10, 11] or EDT-TTF-$CONMe_2$ [12, 13, 14, 15]. These compounds provide a unique possibility for studies of the localization in the quarter-filled one-dimensional band. The question of the localization in 1-D conductors with *tetramerized* stacks is another interesting problem we would like to address here.

For that purpose, we turned our attention to the title compound $(tTTF)_2ClO_4$, based on the asymmetrical electron donor tTTF (trimethylenetetrathiafulvalene). This salt, first reported in 1983 [16] and investigated in more details in 1991 [17] indeed exhibits at room temperature tetramerized 1-D conducting stacks formed by centrosymmetric …BAAB… tetramers of tTTF. It therefore offers an invaluable opportunity to study the effects of charge localization in tetramerized stacks. The $(tTTF)_2ClO_4$ crystals show semiconducting properties with a room temperature conductivity of about 0.1 $\Omega^{-1}cm^{-1}$. At the temperature T = 137 K, an anomaly of the electrical conductivity was observed and had been attributed to a structural phase transition with a superstructure formation, deduced from the onset of superlattice Bragg reflections at the reduced wave vector (0, ½ , ½) for the triclinic unit cell (a = 14.42 Å, b = 6.45 Å, c = 13.35 Å, α = 96.0°, β = 104.9°, γ = 81.9°). Above T = 137 K, quasi-isotropic pretransitional fluctuations were observed – an effect interpreted then as a consequence of interstack coupling. These earlier studies were essentially based on *X*-ray diffuse scattering experiments, transport and EPR

Accepted Manuscript

results; the actual structure of the ClO_4^- salt had not even been determined at room temperature but inferred from its analogy of the unit cell parameters of the isostructural BF_4^- salt. Furthermore, the structure at low temperature, below the phase transition, was not known. Also, asymmetrical TTFs such as tTTF are obtained from the statistical cross-coupling reaction of two different dithiole moieties, enforcing tedious chromatographic separations. The possible contamination with the symmetrical TTF and HMTTF (hexamethylenetetrathiafulvalene) molecules was most probably at the origin of the difficulties encountered then to obtain high quality crystals. In the following, we will describe: *(i)* the preparation of high quality crystals obtained from high purity tTTF molecules, *(ii)* the *X*-ray crystal structures of $(tTTF)_2ClO_4$ at room temperature and 100 K (i.e. well below the 137 K phase transition), and *(iii)* extensive infrared (IR) and Raman studies on monocrystalline samples performed from room temperature (RT) down to about 10 K. These comprehensive investigations will allow us to provide a rationale for the observed phase transition, while signatures of high- and low-temperature states of charge localization in the one-dimensional tetramerized system are identified. An important influence of the ClO_4^- anions on tTTF stacks will be also discussed.

2. Methods

The high-purity donor molecule tTTF was synthesized according to our original procedure described previously for the preparation of $(tTTF)_2X$ (*X* = Cl, Br, I) halide salts [18]. Rather than the NEt_3 coupling of a equimolar mixture of 1,3-dithiolium and 4,5-trimethylene-1,3-dithiolium cations which provides tTTF mixed with symmetric TTF and HMTTF [19, 20], we used the selective Witting-Horner coupling reaction between 1,3-dithiolium-2-dimethylphosphonate and dihydro-4*H*-cyclopenta[d][1,3]dithiol-2-ylidene)piperidinium hexafluorophosphate in the presence of tBuOK, followed by AcOH addition. The tTTF is obtained as sole tetrathiafulvalene derivative. Black plates of $(tTTF)_2ClO_4$ were obtained by electro-crystallization of 10 mg of tTTF at 1µA (galvanostatic mode) in a H-shape electro-crystallization cell containing 12 ml of a 0.05 mol l^{-1} $TBA{\cdot}ClO_4$ / acetonitrile solution.

Single crystal *X*-ray diffraction data were collected at room temperature on an APEXII, Bruker-AXS diffractometer operating with graphite-monochromated Mo-Kα radiation (λ = 0.71073 Å). The structures were solved by direct methods using the *SIR92* program [21] and then refined with full-matrix least-square methods based on F^2 (*SHELXL-2014/7*) [22] with the aid of the WINGX program [23]. All non-hydrogen atoms were refined with anisotropic atomic displacement parameters. H atoms were finally included in their calculated positions.

Accepted Manuscript

Crystallographic data on X-ray data collection and structure refinements are given in table 1. CCDC 1847241 and 1847242 contains the supplementary crystallographic data for this paper. The data can be obtained free of charge from The Cambridge Crystallographic Data Centre via www.ccdc.cam.ac.uk/structures.

Table 1. Crystallographic data for $(tTTF)_2ClO_4$ at T = 278 and 100 K.

	T = 278 K	T = 100 K
CCDC	1847242	1847241
Formula	$C_{18}H_{16}ClO_4S_8$	$C_{36}H_{32}Cl_2O_8S_{16}$
Formula moiety	$2(C_9H_8S_4)$, ClO_4	$4(C_9H_8S_4)$, $2(ClO_4)$
Crystal size	0.16×0.06×0.05	0.16×0.06×0.05
FW (g.mol^{-1})	588.24	1176.47
System	triclinic	triclinic
Space group	P–1	P–1
a (Å)	6.4067(5)	12.641(7)
b (Å)	14.3191(13)	13.954(7)
c (Å)	13.3251(11)	14.158(7)
α (deg)	106.476(3)	102.66(2)
β (deg)	96.097(3)	110.517(19)
γ (deg)	79.934(3)	98.95(2)
V (Å^3)	1152.10(17)	2207(2)
T (K)	278(2)	100(2)
Z	2	4
D_{calc} (g.cm^{-1})	1.696	1.770
μ (mm^{-1})	0.917	0.957
Total refls	34448	44127
θ_{max} (°)	30.54	30.843
Abs corr	multi scan	multi scan
T_{min}, T_{max}	0.936, 0.955	0.933, 0.953
Uniq. refls	6980	13439
R_{int}	0.0586	0.1133
Uniq. refls (I > 2σ(I))	4784	5451
R_1	0.0644	0.0567
wR_2 (all data)	0.2054	0.0567
GOF	1.027	0.943
Res. dens. (e Å^{-3})	1.408, –1.379	0.888, –0.939

Accepted Manuscript

Typical dimensions of samples used in optical measurements were 0.2 x 0.1 x 0.01 mm^3. The optical axes of the $(tTTF)_2ClO_4$ crystals were determined as those displaying the largest reflectance anisotropy. Single-crystal infrared (IR) reflectance spectra in the 100-25000 cm^{-1} frequency range were collected from the (001) crystal face, for IR beam polarized along *b* and *a*-axes, that are parallel and perpendicular to the stacking direction, respectively. The spectra were measured using Bruker IFS 66v/S and a Bruker Vertex 80 Fourier transform spectrometers equipped with: a Hyperion 1000 IR microscope, a set of suitable polarizers, and a CryoVac He-flow cryostat. Depending on the spectral region, the reflectance data were recorded with different spectral resolutions. In the far-infrared range a resolution of 2 cm^{-1}, in the mid-infrared range a resolution of 0.5 cm^{-1}, in the near-infrared and visible ranges a resolution of 4 cm^{-1} were chosen. The absolute values of reflectance were obtained using a silver or gold mirrors as reference. The optical conductivity was calculated by the Kramers-Kronig transformation of the reflectance data [24]. At low frequencies, the data were extrapolated assuming a constant value appropriate for insulators, and at higher frequencies, the data were assumed to decay with a ω^{-2} behavior (up to 10^6 cm^{-1}) and ω^{-4} behavior (above 10^6 cm^{-1}). The samples were mounted on the cold finger with the help of carbon paste.

Raman spectra were measured in a backscattering geometry with a micro-Raman LABRAM HR800 spectrometer. Laser line of the 632.8 nm (He-Ne) was used with power reduced below 0.1 mW to avoid sample overheating. The spectra were recorded with a spectral resolution of 2 cm^{-1}. At room temperature the spectra were measured in the 100 -1700 cm^{-1} frequency range. Variable temperature Raman spectra in the 400 - 600 cm^{-1} and 1300 - 1700 cm^{-1} frequency ranges were measured with a help of a continuous-flow cold finger cryostat manufactured by the Oxford Instruments. A good thermal contact was ensured by vacuum grease. The IR and Raman spectra were collected at several temperatures from room temperature down to 10 K with the cooling rate of about 1 K/min.

The vibrational features in the optical conductivity were decomposed by standard peak-fitting techniques that allow extracting the center frequency and the integral intensity. The bands were fitted using the Voigt spectroscopy function in the PeakFit program [25].

The tight-binding band structure calculations and $\beta_{HOMO-HOMO}$ interaction energies were based upon the effective one-electron Hamiltonian of the extended Hückel method [26], as implemented in the Caesar 1.0 chain of programs [27]. The off-diagonal matrix elements of the Hamiltonian were calculated according to the modified Wolfsberg-Helmholz formula [28]. All valence electrons were explicitly taken into account in the calculations and the basis set

Accepted Manuscript

consisted of double-ζ Slater-type orbitals for all atoms except H (single-ζ). The exponents, contraction coefficients, and atomic parameters for Ni, C, S, N and H were taken from a previous work [29].

The theoretical calculations of normal modes for the tTTF molecule with the charges 0 or +1*e* were performed with Gaussian 03 [30] using the 3-21G basis set and the hybrid Hartree-Fock density functional (B3LYP). The results of the structure optimization correspond to energy minima because no imaginary frequencies were found. The C_S (mirror) symmetry of the molecule was identified at the level of the theory. On the basis of the optimized structure, the vibrational frequencies and Raman activities were calculated. The Raman activity was transformed to Raman intensity [31]. The frequencies computed with a quantum harmonic approximation tend to be higher than the experimental ones. The scaling factor 0.9614 was used [32].

3. Results

3.1. Crystal (and band) structures of $(tTTF)_2ClO_4$

At room temperature (RT), $(tTTF)_2ClO_4$ crystalizes in the triclinic system, space group $P\bar{1}$, with two tTTF molecules in general position in the unit cell (figure 1) and one ClO_4^- anion, disordered on two positions with an approximate 2/3-1/3 distribution (Supplementary Material - figure S1). It is isostructural with the BF_4^- salt described earlier [16]. Since we are in the presence of two crystallographically independent tTTF molecules, the exact individual charge might differ from the average +0.5*e* value. Bond distances within the TTF core are usually excellent indicators of the charge as the oxidation is systematically accompanied by a lengthening of the central C_i=C_i inner double bond and a shortening of the C_i–S single bonds. These values are reported in table 2, together with those of reference compounds. In the absence of structures for the neutral tTTF and fully oxidized tTTF salts (ρ = 1), it is not possible to establish a useful correlation between the C_i=C_i, C_i–S bond distances and the charge, as usually done. We note however that the C_i=C_i and C_i–S bond distances in both molecules A and B are very close to those reported for $(tTTF)_2Br$ with one crystallographically independent molecule of an unambiguous ρ = 0.5 charge, with eventually a weak tendency for higher charge ($0.5+\delta_1$) for molecule A. In the crystal, the two molecules are associated into inversion-centered tetramers (BAAB) with typical bond-over-ring overlap within the tetramers, and a shifted overlap between tetramers (figure S2). Calculations of the $\beta_{HOMO\text{-}HOMO}$ overlap interaction energies confirm stronger AA and AB interactions within the (BAAB) tetramers (β_{AA} = 0.700

Accepted Manuscript

eV, β_{AB} = 0.682 eV), and much weaker BB interactions β_{BB} = 0.049 eV) between tetramers along the stacking axis.

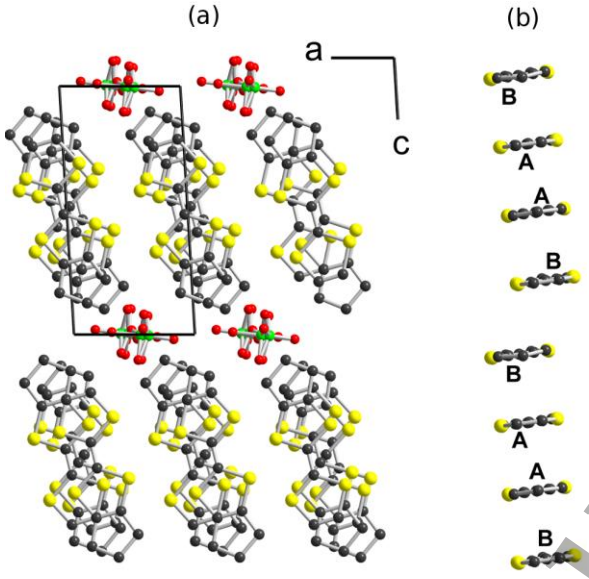

Figure 1. Structure of $(tTTF)_2ClO_4$ at room temperature: (a) Projection view of the unit cell along *b*-axis; (b) Detail of the inversion-centered (BAAB) tetramers stacking along *b*-axis.

The 137 K transition had been tentatively associated with an ordering of the ClO_4^- anions (see below). The structure collected at T = 100 K is solved in a double unit cell, in the triclinic system, space group $P\bar{1}$, with now four tTTF molecules (A-D) in general position in the unit cell, and two different, non-disordered ClO_4^- anions (figure 2). Altogether the structural changes within the tTTF stack appear very limited: the four tTTF molecules still organize into (ABCD) tetramers with typical bond-over-ring overlap within the tetramers, and a shifted overlap between tetramers (figure S3), as observed at RT. Based on the evolution of C_i=C_i and C_i–S bond lengths (table 2), the deviation from the averaged +0.5*e* charge within each of the four A-D tTTF molecules is now larger than that at RT, with A and D less oxidized (ρ = 0.5–δ_2), B and C more oxidized (ρ = 0.5+ δ_2), and $\delta_2 > \delta_1$. In the absence of reference structural data for the neutral tTTF or the fully oxidized (ρ = 1) tTTF salt, it is not possible to estimate here a δ_2 value. The charge separation within the ABCD tetramers (0.5 – δ_2, 0.5 + δ_2, 0.5 + δ_2, 0.5 – δ_2), with a charge concentration on BC molecules at the tetramer center, enhances when compared to that observed at room temperature in the (BAAB) tetramer (0.5 – δ_1, 0.5 + δ_1, 0.5 + δ_1, 0.5 – δ_1). Calculations of the $\beta_{HOMO\text{-}HOMO}$ overlap interaction energies in the 100 K structure gives within the tetramers β_{AB} = 0.662 eV, β_{BC} = 0.791 eV, β_{CD} = 0.718 eV, with the intertetramer overlap interaction at β_{AD} = 0.075 eV. We note therefore, from room temperature

Accepted Manuscript

to 100 K, a parallel strengthening of the central tetramer interaction, associated with this larger charge concentration on the BC molecules.

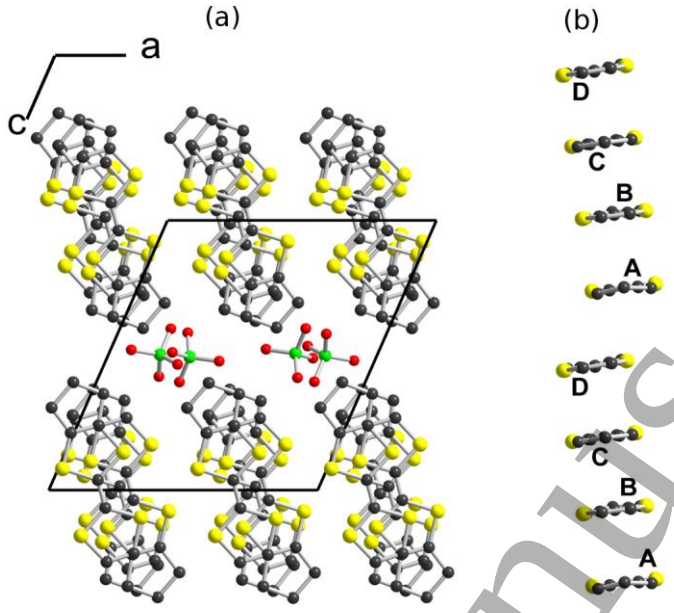

Figure 2. Structure of $(tTTF)_2ClO_4$ at T = 100 K. (a) Projection view of the unit cell along *b*-axis; (b) Detail of the (ABCD) tetramers stacking along *b*-axis.

Table 2. Relevant bond distances in the tTTF core.

	T(K)	ρ	C_i=C_i (Å)	Av. Ci–S (Å)	Ref.
$(tTTF)_2Br$	293	0.5	1.370(3)	1.743(1)*	[18]
$(tTTF)_2ClO_4$	293				this work
Mol. A		$0.5+\delta_1$	1.374(4)	1.734(2)*	
Mol. B		$0.5-\delta_1$	1.371(4)	1.742(2)*	
$(tTTF)_2ClO_4$	100				this work
Mol. A		$0.5-\delta_2$	1.369(20)	1.748(6)*	
Mol. B		$0.5+\delta_2$	1.374(20)	1.737(6)*	
Mol. C		$0.5+\delta_2$	1.377(20)	1.736(6)*	
Mol. D		$0.5-\delta_2$	1.368(20)	1.744(6)*	
tTTF•TCNQ	?	≈ 0.70	1.373(10)	1.738(15)	[33]

* Esd on the averaged C_i–S distances are determined with error propagation rules.

Accepted Manuscript

Band structure calculations were performed based on the crystallographic position determined at RT and T = 100 K (figure 3). With the 2:1 stoichiometry of the $(tTTF)_2ClO_4$ salt, the system is 3/4-filled, leading to a presence of a band gap at both temperatures, in accordance with the semiconducting behavior of the salt. Note that the 100 K structure leads to a notably larger gap (0.11 *vs.* 0.06 eV), a possible explanation for the increased activation energy observed below the T = 137 K phase transition.

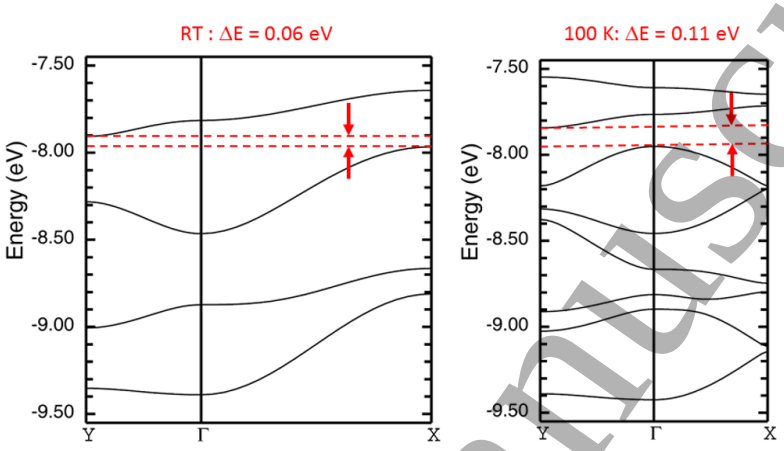

Figure 3. Calculated band structure for $(tTTF)_2ClO_4$ at room temperature (left) and 100 K (right). The red dotted lines delineate the filled and empty bands.

3.2. Polarized reflectance spectra of $(tTTF)_2ClO_4$

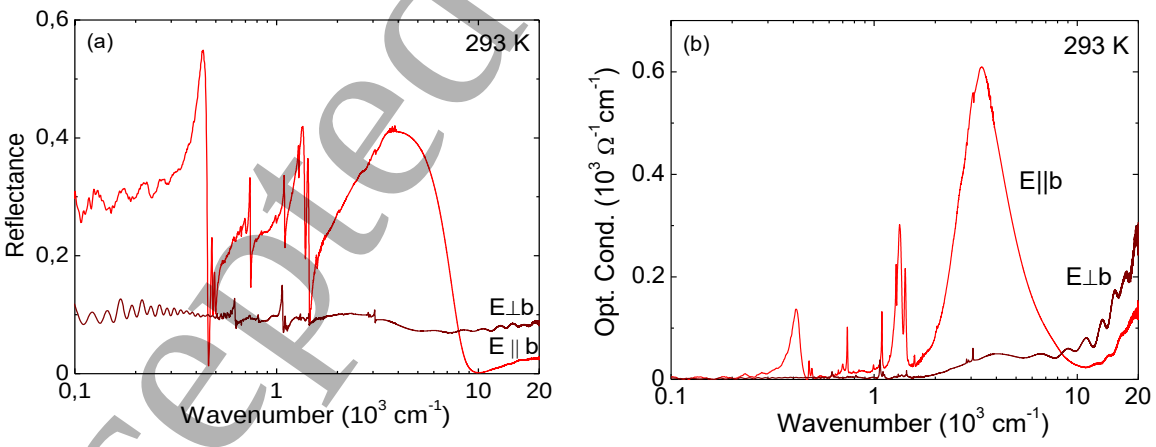

Figure 4. Room temperature polarized reflectance spectra of $(tTTF)_2ClO_4$ (a) and optical conductivity spectra (b) as derived by Kramers-Kronig transformation (note the logarithmic frequency scale).

Accepted Manuscript

Figure 4a displays the RT reflectance spectra of $(tTTF)_2ClO_4$ taken from the (001) crystal face in the frequency range 100-20000 cm^{-1}, polarized parallel and perpendicular to the stacking *b*-axis. Small oscillations of the reflectance observed at low and high frequencies in both polarizations are due to the relatively small thickness of the $(tTTF)_2ClO_4$ samples. The optical conductivity obtained by Kramers-Kronig transformation of the reflectance is shown in figure 4b. The anisotropy of the spectra implies that the electronic structure of $(tTTF)_2ClO_4$ is one-dimensional with significant hopping integrals between tTTF molecules within the stack. The spectrum for E || *b* reveals a semiconducting behavior with a broad electronic absorption centered at about 3700 cm^{-1} and some strong vibrational features below about 1650 cm^{-1} mainly related to the interaction of C-S and C=C modes of tTTF with electrons (e-mv coupling), respectively [34, 35, 36]. The electronic absorption is related to electronic charge transfer transitions between tTTF moieties within the tetramers. Additionally, for E || *b* some bands attributed to the IR active modes of tTTF are seen. The spectrum for E ⊥ *b* is flat with the average reflectance level of about 0.1; for this polarization neither the e-mv coupling features nor IR active modes are found. The weakness of IR active modes for E ⊥ *b* is due to the specific orientation of molecules against the (001) crystal face and the lack of e-mv effects. On the other hand, for this polarization some bands related to ClO_4^- anions are found in the range 1060 - 1120 cm^{-1}.

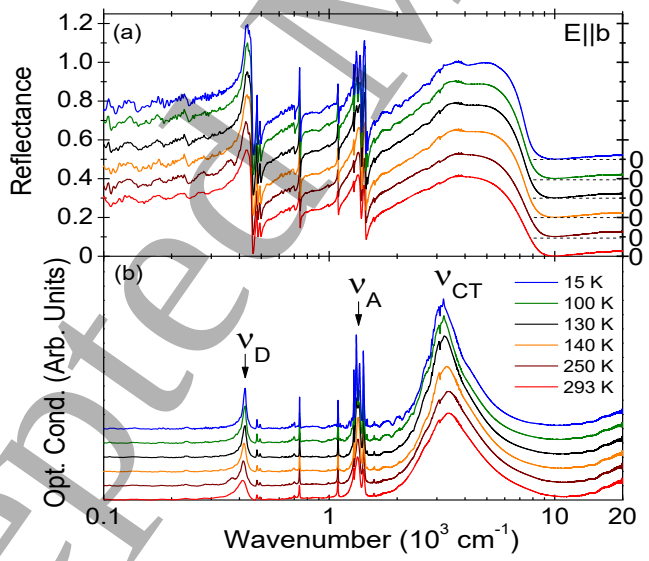

Figure 5. Reflectance (a) and optical conductivity (b) spectra of $(tTTF)_2ClO_4$ for polarization parallel to the stacks at selected temperatures (note the logarithmic wavenumber scale).

Upon decreasing temperature the spectra undergo gradual modifications as demonstrated in figure 5: the oscillation strength of both electronic and vibrational bands increases. The broad

Accepted Manuscript

electronic absorption centered at 3700 cm^{-1} consist of two strongly overlapping components at about 3300 and 4900 cm^{-1} at room temperature; they undergo no important modifications upon decreasing temperature – the only change is a small increase of their intensities (figure S4). These bands are assigned to intra-tetramer charge-transfer excitations, i.e. transitions between molecules A →B and A →A. The inter-tetramer interactions are much smaller but they cannot be neglected, therefore the transition B →B should be also seen in the electronic spectra; it can be hidden in the high-frequency wing of the broad electronic absorption. However, because of its smaller intensity, we are not able to identify unambiguously this electronic feature.

Changes within the charge-transfer band can be related to a redistribution of the spectral weight. In this case the electronic structure of the charge-transfer salt is modified. The evolution of the optical conductivity spectra can be investigated by looking at center of the spectral weight defined as:

$$\langle \omega \rangle = \int_{\omega_1}^{\omega_2} \sigma(\omega)\omega d\omega \Big/ \int_{\omega_1}^{\omega_2} \sigma(\omega) d\omega \qquad (1)$$

where σ is the optical conductivity, ω_1 and ω_2 are the integration limits. In the spectra of $(tTTF)_2ClO_4$ with polarized light E || b in the 120 - 150 K temperature range $\langle\omega\rangle$ shifts significantly toward low frequencies (figure 6). The center of the spectral weight is about 4300 cm^{-1} in the 150 - 293 K temperature range and is about 4000 cm^{-1} at the lowest temperatures. It demonstrates that the redistribution of the spectral weight affects the shape of the charge-transfer band at the phase transition temperature. This modification is due to decrease of the inter-tetramer interactions and consequently the charge localization within tTTF tetramers.

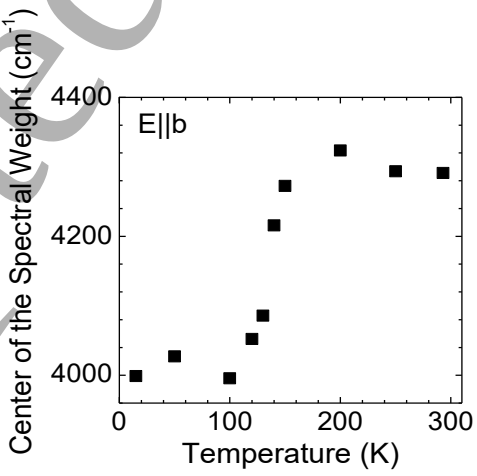

Figure 6. Temperature dependence of the center of the spectral weight in the 100-10000 cm^{-1} frequency range for the spectra of $(tTTF)_2ClO_4$ polarized parallel to the stack.

Accepted Manuscript

In the spectrum for E || *b* the most prominent IR oscillation features are due to interactions between the C=C stretching modes of tTTF and electrons (figure 7a). The coupling of intramolecular vibrations with electronic background (e-mv coupling) induces a dipole moment oscillating along the stacking axis, yielding thus strong and broad bands. Taking into account the stacking structure, it is reasonable to discuss the vibrational spectra of $(tTTF)_2ClO_4$ within a model of quasi-isolated BAAB tetramers. The structural data of the $(tTTF)_2ClO_4$ indicate a non-uniform charge distribution among molecules inside tetramers suggesting that the charge residing on the central A molecules is larger than that on B molecules, yielding a charge pattern with …0110… periodicity. Therefore, we suggest to consider the vibrational tetrameric modes as a combination of two dimeric modes, similarly as recently discussed for the low-temperature phase of TMTTF salts with tetrahedral anions [37]. For an isolated tetramer there exist four tetrameric modes. Two tetrameric modes constitute a dimeric mode corresponding to the in-phase oscillations of monomers in dimers BA and AB, i.e. they are composed of in-phase (*gg*) and out-of-phase (*gu*) oscillations of these dimers within tetramer. The two other tetrameric modes form a dimeric mode corresponding to the out-of-phase oscillations of monomers in dimers BA and AB, i.e. they consist of symmetric (*uu*) and anti-symmetric (*ug*) oscillations of dimers in relation to the tetramer center. For centrosymmetric molecules the modes *gg* and *uu* are Raman active since the charge density moves symmetrically and no dipole moment is produced. The effect of e-mv coupling is observed for the modes *gu* and *ug* because they yield the dipole moment oscillations and thus IR features, polarized along the stacking axis. However, as the tTTF donor has no center of symmetry, both *gg* and *uu* modes can be observed in IR spectra, too.

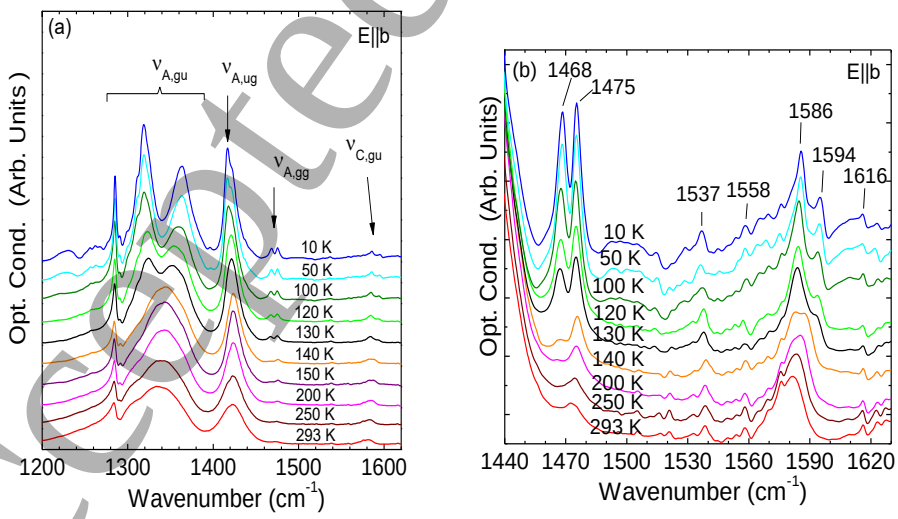

Figure 7. Optical conductivity in the region of C=C stretching modes for polarization E || *b* (a); vibrational details in the region 1450-1630 cm^{-1} (b).

Accepted Manuscript

Usually, in the case of charge-transfer salts formed by TTF derivatives, the attention is focused on the C=C stretching vibrations of the TTF derivatives since these modes are most sensitive for the charge residing on molecules, providing thus a possibility of evaluation of the charge distribution on molecules [35, 38]. On the other hand, these modes strongly couple with the electronic system yielding strong and broad e-mv bands in IR spectra. Recently, it was shown that also ring breathing C-S stretching modes can be useful for studies of charge distribution and they can give additional complementary information [39]. A schematic view of the three C=C and two C-S modes of $tTTF^{+}$ cation is shown in figure 8. The detailed results of our DFT calculations and assignment of vibrational bands of $(tTTF)_2ClO_4$ are given in table S1. Since tTTF has no center of symmetry, all these modes are both IR and Raman active. In vibrational spectra of neutral $tTTF^{0}$ molecule we have observed these modes at the following frequencies: ν_A= 1520 cm^{-1}, ν_B= 1550 cm^{-1}, ν_C= 1612 cm^{-1}, ν_D= 467 cm^{-1}, ν_E= 415 cm^{-1}.

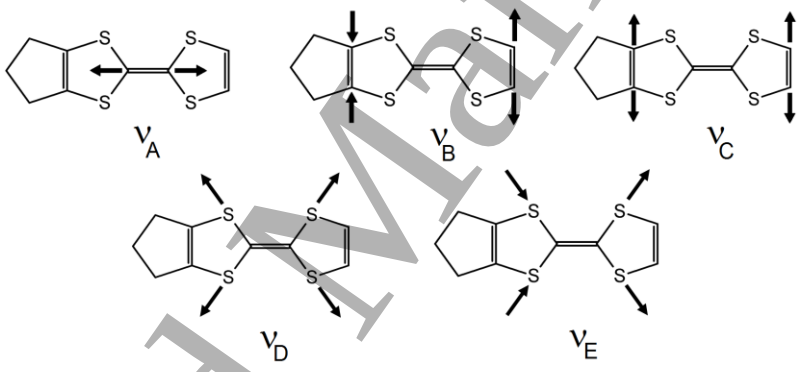

Figure 8. Normal modes of $tTTF^{+}$ cation related to C=C and C-S vibrations.

A broad band centered at about 1340 cm^{-1} at 296 K is a spectral consequence of the e-mv coupling of the central C=C stretching mode ν_A (figure 7a). We assign this band to the tetrameric *gu* mode ($\nu_{A,gu}$). On the wing of the intense vibronic absorption a strong dip structure at about 1290 cm^{-1} is located, attributed to a C-H bending vibration of tTTF. It is usual for organic conductors based on TTF derivatives that the C-H mode appears in as an antiresonance dip superimposed on the wing of the broad C=C band [35, 40]. Additionally, we also relate the strong e-mv coupling feature at 1430 cm^{-1} to the central C=C stretching ν_A vibration, namely the tetrameric $\nu_{A,ug}$ mode. On decreasing temperature, both e-mv bands get sharper and split below the phase transition temperature 137 K, providing evidence of non-uniform charge distribution inside tetramers (figure 7a). The splitting is very well seen for the $\nu_{A,gu}$ band but it is also present for the $\nu_{A,ug}$ band, though in this case the components are much less separated

Accepted Manuscript

(1417 and 1422 cm^{-1} at 10 K) . Several other weaker IR features assigned to the C=C modes are also observed above 1450 cm^{-1} (figure 7b). The band at 1473 cm^{-1} at RT is to be assigned to the $\nu_{A,gg}$ mode which is IR active in the case of tTTF; below 137 K it yields a doublet structure at 1468 and 1475 cm^{-1}. A rather broad band at about 1582 cm^{-1} can be related to the $\nu_{C,gu}$ mode which splits into two lines at 1586 and 1594 cm^{-1} below 137 K. The observed doublet structure of these C=C bands is due to non-uniform charge distribution in the tetramers. In a small temperature range above 137 K some pre-transitional effects can be identified. All the IR bands assigned to the C=C stretching modes together with proposed assignments are listed in table S2.

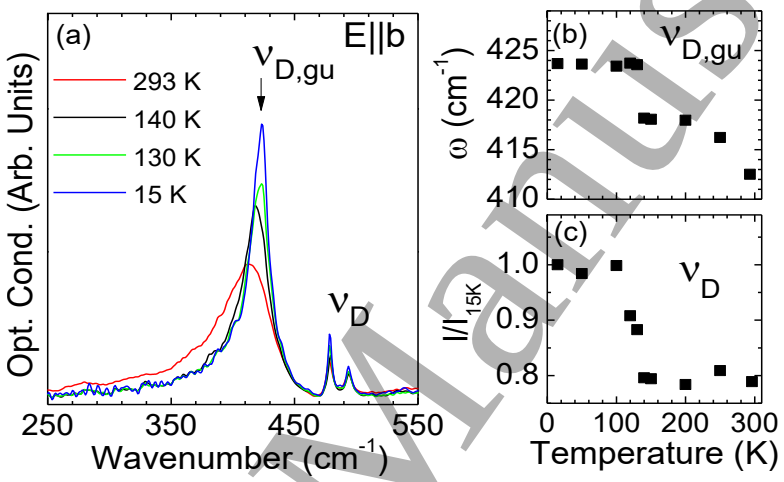

Figure 9. (a) Polarized IR optical conductivity spectra of $(tTTF)_2ClO_4$ in the 250-550 cm^{-1} frequency range; the temperature evolution of the frequency of the $\nu_{D,gu}$ band (b) and normalized intensity of the two-component ν_D band observed in the optical conductivity spectra (c).

In the low-frequency part of the IR spectrum a broad band centered at about 450 cm^{-1} due to e-mv coupling of the ν_D mode is seen (figure 9a). We relate this band to the tetrameric $\nu_{D,gu}$ mode, though it can also be a superposition of $\nu_{D,gu}$ and $\nu_{D,ug}$ modes; this band also consists of several components. Due to the phase transition it slightly shifts towards higher wavenumbers (figure 9b) and its intensity increases. Two much weaker and narrower bands at 479 and 493 cm^{-1} are assigned to $\nu_{D,uu}$ and $\nu_{D,gg}$ terameric modes, which should exhibit the IR activity for the asymmetrical tTTF donor (figure 9c). The tetrameric mode of *uu* symmetry involves charge oscillation between monomers, therefore it is reasonable to assume that it has

Accepted Manuscript

a lower frequency. On closer examination of these bands below T = 137 K one can find that both bands show a weak doublet structure: 472 and 479 cm^{-1}, 486 and 493 cm^{-1}, respectively.

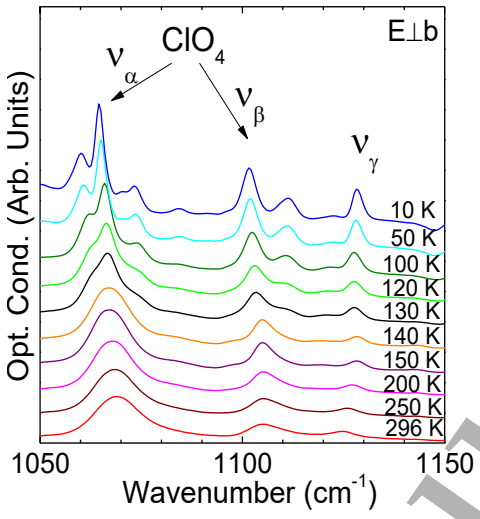

Figure 10. Optical conductivity spectra of $(tTTF)_2ClO_4$ polarized perpendicular to the stack in the 1050 -1150 cm^{-1} frequency range at selected temperatures.

As already mentioned above, due to the special orientation of molecules against the (001) crystal face, the bands related to IR active vibrations of tTTF are only well observed for polarization E || b. Nevertheless, for polarization E ⊥ *b* we find relatively broad bands at around 1069 and 1105 cm^{-1} at T = 293 K related to the IR active mode of the ClO_4^- anion, denoted as ν_α and ν_β, respectively (figure 10). In the close neighborhood we find another band at 1125 cm^{-1} denoted as ν_γ. Below 137 K both bands ν_α and ν_β get sharper and split into four and two components, respectively, while the band ν_γ remains a single line (details of the analysis are displayed in figure S5). The notable splitting of the bands ν_α and ν_β is to be related with the anion ordering transition which – as already suggested by the structural data – is intimately correlated with the reorganization of tTTF stacks.

3.3. Raman spectra of $(tTTF)_2ClO_4$

In order to gain deeper insight into the charge distribution on tTTF molecules and its modifications due to stack reorganization in the $(tTTF)_2ClO_4$ salt, we have also performed investigations of the Raman spectra as a function of temperature.

Accepted Manuscript

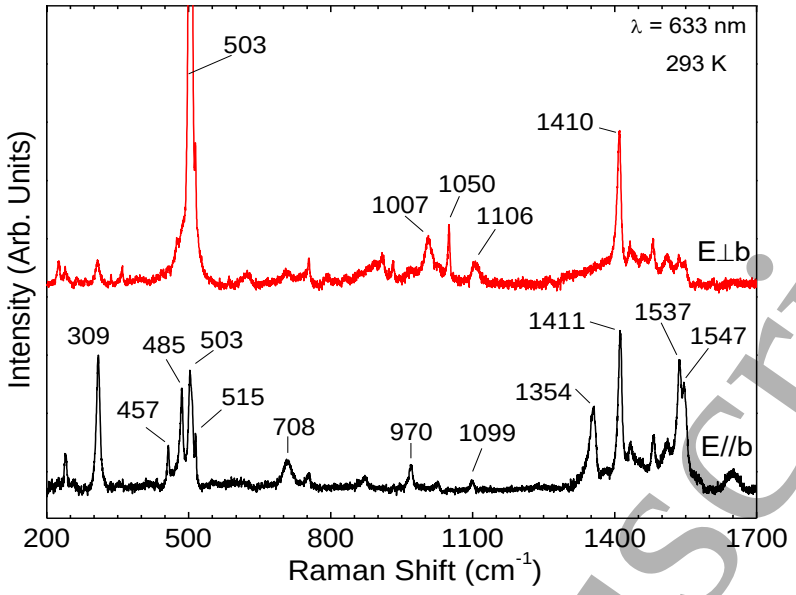

Figure 11. Room temperature Raman spectra of $(tTTF)_2ClO_4$ measured for the electrical vector of polarized laser light parallel (E || b) and perpendicular (E ⊥ *b*) to the stacking *b*-axis.

Raman spectra of $(tTTF)_2ClO_4$ at room temperature (RT) were measured in the frequency range 100 - 1700 cm^{-1} with incident laser light polarized parallel (E || b) and perpendicular (E ⊥ *b*) to the stacks (figure 11). The band assignment was performed on basis of the vibrational spectra of salts formed by similar DMtTTF [10] and tTTF-I [41] donors, as well as our results of DFT calculations (figure S6 and table S1). Surprisingly, at T = 293 K in the spectrum of $(tTTF)_2ClO_4$ for polarization E || b, one can clearly see bands assigned to the fully ionized $tTTF^{+1}$ cations: at 1411 cm^{-1} (ν_A mode) and a doublet at 1537 and 1547 cm^{-1} (ν_C mode). Additionally, we propose that two Raman features at 1355 and 1433 cm^{-1} are a result of the e-mv coupling of ν_A and ν_C modes, respectively, i.e. the bands observed in IR spectra are also seen in Raman spectra, though their intensity is much smaller. The appearance of the $tTTF^{+1}$ bands is a consequence of strong charge fluctuations in conducting stacks; the life time of $tTTF^{+1}$ ions should be rather short but comparable with the time-scale of vibrational spectroscopy. It is important to note that at RT the bands of $tTTF^{+1}$ are much stronger in comparison to those attributed to $tTTF^{+0.5}$. Evidently, at ambient temperature the charge fluctuations in stacks are so strong that they yield a quite large density of $tTTF^{+1}$ cations. This conclusion is also supported by the spectral data in the frequency range of the C-S ring breathing modes, where one can find three features at 485, 503, and 515 cm^{-1} related to the ν_D vibrations of molecules with charges 0, +0.5*e*, +1*e*, respectively. Analogously, as proposed for C=C modes, we suggest that a feature at 457 cm^{-1} is due to the e-mv coupling of ν_D mode. For E ⊥ *b*

Accepted Manuscript

the spectral features attributed to the effect of e-mv coupling are not seen, as should be expected for this polarization, and other bands appear with different intensities because of the specific orientation of tTTF molecules against the (001) crystal face.

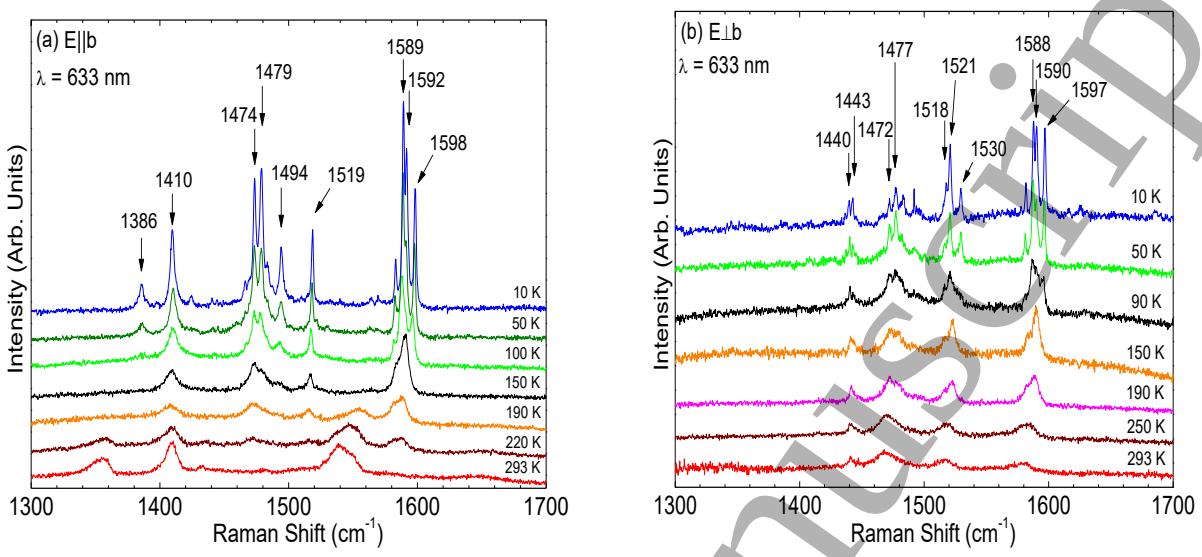

Figure 12. Raman spectra of $(tTTF)_2ClO_4$ measured with exciting laser light polarized (a) parallel E || b and (b) perpendicular E ⊥ *b* to the stacks in the 1300-1700 cm^{-1} frequency range at selected temperatures.

Figure 12 shows the temperature evolution of the Raman spectra of $(tTTF)_2ClO_4$ in the frequency region 1300-1700 cm^{-1} for both polarizations. At RT, for E || b the spectrum is dominated by the broad C=C bands of $tTTF^{+1}$ cations because of the strong charge fluctuations (figure 12a). On cooling down the intensity of $tTTF^{+1}$ bands gradually decreases, indicating that the charge fluctuations get weaker, and the ν_C band shifts towards higher wavenumbers. The shift of the ν_C band can be related with a decrease of the average charge on the cations. An analogous effect is not observed for the ν_A mode since it couples much stronger with electrons. Yamamoto and Yakushi [42] showed that for radical cation tetramers with large e-mv coupling constants the frequency of the Raman active in-phase tetrameric mode is nearly independent on the charge distribution among the molecules in a tetramer and that it corresponds to the average charge residing on tetramer moieties. The frequency shift of this mode is only observed in the case of weak e-mv coupling. In our case, taking into account suitable data for TTF and its derivatives [35, 36], it is reasonable to assume that the e-mv coupling constant for the ν_A mode is much larger than the one for the ν_C mode, therefore only the ν_C band shows frequency shift due to decrease of the charge density fluctuations in the stacks when the crystal is cooled down.

Accepted Manuscript

Simultaneously, the intensities of bands attributed to molecules with charge about +0.5*e* are growing, so that at 150 K we clearly see features related to $tTTF^{+0.5}$ at 1473 cm^{-1} (ν_A mode), 1518 cm^{-1} (ν_B mode) and 1591 cm^{-1} (ν_C mode). Moreover, we also observe the ν_A band of $tTTF^{+1}$, which grows again, but the ν_C band of $tTTF^{+1}$ completely decays. Below the phase transition at 137 K the ν_A and ν_C bands of $tTTF^{+0.5}$ increase their intensities and split (figure S7), while the ν_B remains a single line down to the lowest temperatures. Individual components of the split lines are attributed to various tetrameric modes (see table S3). On the other hand, for polarization E ⊥ *b* the RT spectrum is dominated by three broad features centered at about 1474, 1519 and 1589 cm^{-1} assigned to ν_A, ν_B, and ν_C modes of $tTTF^{+0.5}$, respectively (figure 12b). Surprisingly, for this polarization only one band related to $tTTF^{+1}$ cations is found, namely the ν_B mode at 1440 cm^{-1}. For E ⊥ *b* the band intensities grow with temperature decreasing and below the phase transition the bands split. Some pre-transitional spectral effects are also seen in a small temperature range above 137 K. The most important Raman bands together with the proposed assignment are collected in table S3.

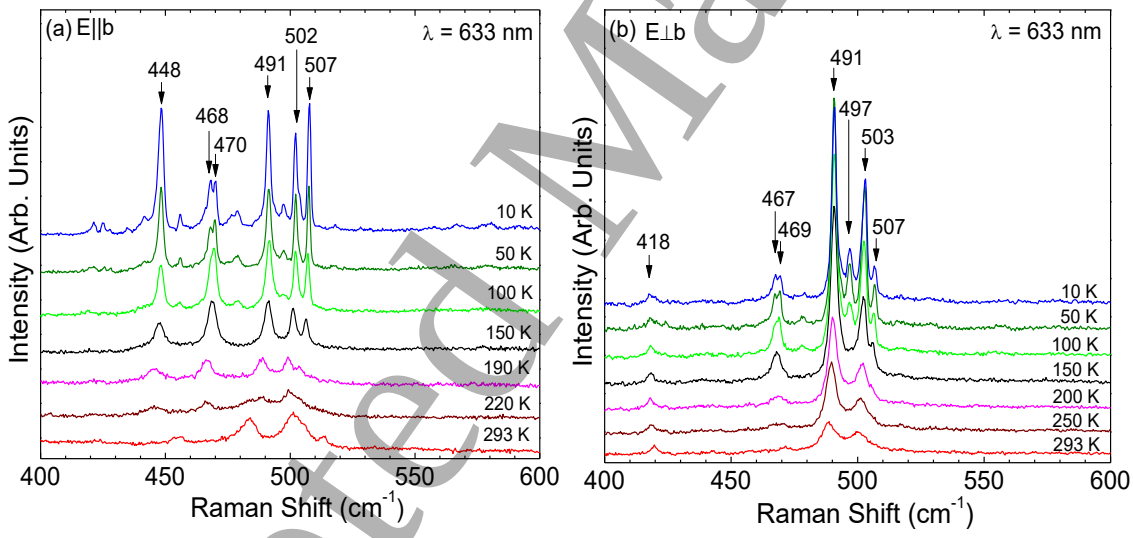

Figure 13. Raman spectra of $(tTTF)_2ClO_4$ measured with incident light (a) parallel E || b and (b) perpendicular E ⊥ *b* to the stacks in the 400 - 600 cm^{-1} frequency range at selected temperatures.

As mentioned above, the C-S stretching ring breathing vibrations are also very useful for studying modifications of the charge distribution in the conducting stacks. Figure 13a presents Raman spectra of $(tTTF)_2ClO_4$ in the region of ring breathing modes for polarization

Accepted Manuscript

parallel to the stacking direction (E || b). At RT broad bands centered at about 485, 503 and 515 cm^{-1} can be assigned to the ν_D mode of molecules with charges 0, +0.5*e*, and +1*e*, respectively. As the temperature is decreasing, the intensity of these bands decreases and the charge distribution in stacks evidently undergoes a reorganization. Just above the phase transition, at 150 K for E || b we see three bands which we propose to attribute to the tetrameric $\nu_{D,uu}$ mode at 491 cm^{-1} and $\nu_{D,gg}$ mode at 501 and 506 cm^{-1}. Evidently, the doublet structure of $\nu_{D,gg}$ mode is due to non-uniform charge distribution in tTTF tetramers. Below the phase transition at 10 K we see that both tetrameric modes are doublets. The broad feature at 457 cm^{-1} at RT, related to the effect of e-mv coupling of ν_D mode, disappears at 150 K. The other Raman bands seen at 10 K can be assigned to the ν_E mode at 448 cm^{-1} and the ClO_4^- anions (467 and 469 cm^{-1}) – for details see table S3.

For the polarization E ⊥ *b* at RT we observe two broad ν_D bands centered at about 489 and 500 cm^{-1}, which we relate to molecules with charges 0 and +0.5*e*, respectively. These bands decrease their intensities on cooling down (figure 13b) and a new structure gradually grows. So that at 10 K there are two doublets related to the tetrameric modes: $\nu_{D,gg}$ (502 and 507 cm^{-1}) and $\nu_{D,uu}$ (491 and 497 cm^{-1}). As already suggested above, the mode splitting is a consequence of non-uniform charge distribution in tetramers. Moreover, we observe the band of ClO_4^- which at 10 K shows a doublet structure at 467 and 469 cm^{-1}. This doublet structure is similar to that for E || b. The bands observed for polarization E ⊥ *b* are also listed in table S3.

4. Discussion

The above presented temperature evolution of both the Raman and IR spectra shows that the charge distribution fluctuates in the tTTF stacks and undergoes significant modifications. Formally, each tTTF has a charge of +0.5*e* but vibrational features of molecules with different charges are clearly observed down to the lowest temperatures. The Raman spectra indicate that close to RT the charge fluctuations in the tTTF stacks are responsible for the appearance of strong and broad bands of molecules with charge +1*e*. The life-time of the $tTTF^{+1}$ cations is sufficiently long to be observed by vibrational spectroscopy methods. At RT we see the three C=C modes of $tTTF^{+1}$: ν_A (1409 cm^{-1}) and ν_C (1540 cm^{-1}) for E || b, and ν_B (1440 cm^{-1}) mode for E ⊥ *b*, while the C=C bands related to vibrations of the $tTTF^{+0.5}$ molecules are much weaker. The effect of the charge fluctuations is also found in the region of the ring-breathing

Accepted Manuscript

C-S modes, where we clearly see the ν_D bands assigned to molecules with charges: 0, +0.5*e*, and +1*e*. On cooling down the ν_A and ν_C bands of TTF^{+1} decrease their intensities, indicating that the amplitude of charge fluctuations weakens. Simultaneously, the frequency of the ν_C band grows, though the position of the ν_A band does not change. As discussed above, this effect is attributed to the different strength of the e-mv interactions. The shift of the ν_C mode is due to decrease of the average charge residing on the charge-rich molecules in the stacks – on cooling this charge gradually approaches the formal value of +0.5*e* per molecule. The strength of charge fluctuations is directly related with the decrease of charge carrier density in conduction band on temperature decreasing. The IR spectra provide also evidence of charge fluctuations because some $tTTF^{+1}$ bands can be identified, while they are not so obvious as in Raman spectra. Our spectroscopic data do not provide any indication of non-uniform charge distribution among the molecules in tetramers above the phase transition temperature. Due to charge fluctuations the bands are too broad to distinguish any structure; we cannot rule out that it is hidden.

Below the phase transition temperature at 137 K, the charge is localized in tetramers and evidently it is distributed non-uniformly among tTTF molecules, as indicated by both IR and Raman data. The degree of splitting of various vibrational bands can be used to evaluate the charge density distribution. Obviously, not all modes are suitable for such evaluation since those strongly interacting with electrons may give less reliable values of the charge density. On basis of our Raman data we roughly estimate that for the fully ionized tTTF molecule, the ν_c mode shifts towards lower wavenumbers by about 90 -100 cm^{-1}, whereas the ν_D mode shifts by about 30 cm^{-1} towards higher wavenumbers. Taking into account these data and the values of the band splitting for the $\nu_{A,gg}$ and $\nu_{D,gg}$ bands (see table S3) we estimate that in the low-temperature phase the charge deviates from the formal charge +0.5*e* by $\delta_2 \approx +0.05e$ and +0.08*e*, respectively. In agreement with the structural data, we suggest that molecules with higher charge density are located in the center of the tetramer, i.e. on B and C molecules. Unfortunately, because the strong charge fluctuations make the bands very broad, we are not able to perform an analogous estimation for the high-temperature phase.

It is important to note that down to the lowest temperature we can identify bands attributed to $tTTF^{+1}$ cations both in IR (ν_B and ν_C modes) and Raman (ν_A and ν_B modes) spectra. However, there is an important difference between effects responsible for appearance of the $tTTF^{+1}$ cations in the high- and low-temperature phases. We propose that close to room temperature the charge is *delocalized* in tTTF stacks and undergoes strong fluctuations. A consequence of these fluctuations is that in the time-scale of vibrational spectroscopy charge-rich and charge-poor sites are accidentally formed in the stacks. At RT we see that the charge-

Accepted Manuscript

rich sites have a charge of about +1*e* but - as indicated by the shift of the ν_c mode - on cooling the charge-rich sites have smaller and smaller charge, gradually approaching the value of +0.5*e*. Evidently, the fluctuations and thus the degree of charge difference between charge-rich and charge-poor sites are decreasing. On the other hand, in the low-temperature phase, the charge is *localized* in the tTTF tetramers but it is distributed non-uniformly among monomers, therefore, we see again the bands attributed to molecules with charge +1*e*, located in positions B and C. Analyzing the temperature dependence of the band intensities we estimate that the process of localization in tetramers begins at about 150 – 180 K, i.e. above the phase transition temperature 137 K, in agreement with previously observed pre-transitional phenomena [17]. Below 137 K the life-time of $tTTF^+$ cations is long enough to be observed in our experiments but it is not sufficiently long to form relatively long-living doubly charged $(tTTF^+)_2$ dimers. Therefore, in IR spectra down to the lowest temperatures we observe no charge-transfer absorption band assigned to transition between two charged molecules and thus no IR feature related to coupling of vibrational modes with such transition.

Let us recapitulate what is known for related low-dimensional charge transfer salts. The most intensely studied group of one-dimensional organic conductors with tetramerized stacks were 1:2 charge-transfer salts formed by the acceptor TCNQ (tetracyano-quinodimethane) with the following cations: TEA [43], MTPP [44], NPrQn [45], PrPht [46] and PrQiun [47]. Depending on the cation, the TCNQ stacks exhibit slightly different organization, i.e. different value of both intra- and inter-tetramer interactions, which is directly related with conducting properties. It was shown, mostly by IR studies, that in these salts a non-uniform charge distribution usually exists inside centrosymmetric ABBA tetramers and it undergoes modifications as a function of temperature [48, 49, 50, 51, 52]. This conclusion was mainly based on the observation of the splitting of the IR bands attributed to the coupling of the totally symmetric (A_g) TCNQ vibrational modes with the charge-transfer excitations. The doublet structure of vibrational modes was interpreted as a consequence of charge localization. Narrow split bands were interpreted as a consequence of the e-mv coupling of totally symmetric TCNQ modes of Ag symmetry with charge-transfer transition between two charged molecules (BB molecules in tetramers) located at about 8000-9000 cm^{-1} [52]. In tetramerized TCNQ salts the life-time of $TCNQ^{-1}$ anions is long enough to create sufficiently long-living doubly charged $(TCNQ^-)_2$ dimers and thus the presence of the electronic excitation at 8000-9000 cm^{-1}.

The charge localization effects in $(tTTF)_2ClO_4$ are notably different in comparison with prototypical tetramerized TCNQ salts. Firstly, strong charge fluctuations in the high-temperature phase of $(tTTF)_2ClO_4$, which are responsible for appearance of molecules with

Accepted Manuscript

charge +1*e*, were not observed in TCNQ salts. Secondly, in the low-temperature phase of $(tTTF)_2ClO_4$ localization inside tetramers is weaker than in TCNQ salts, therefore no charge-transfer transition between two charged molecules is found. On the other hand, due to localization in tetramers in $(tTTF)_2ClO_4$ we see a clear splitting of the IR feature related to the coupling of the ν_A mode with the charge-transfer transition between charged and neutral molecule. Thirdly, in the vibrational spectra $(tTTF)_2ClO_4$ we can clearly distinguish different tetrameric modes. The tetrameric modes, probably for the first time, were clearly observed in the salts $(TMTTF)_2X$ (X=BF_4, ClO_4, ReO_4), in which the teramerization is related with the anion ordering transition. However, bands assigned to the $v_3(a_g)$ and $v_4(a_g)$ modes of $TMTTF^+$ cations, analogous to v_C and v_A vibrations of $tTTF^+$, were not seen [37]. It means that the charge fluctuations in the high-temperature phase of TMTTF salts are much weaker. In conclusion, the salt $(tTTF)_2ClO_4$ is a special case of one-dimensional tetramerized organic conductor.

To shed some light on the electronic states of $(tTTF)_2ClO_4$ in the high- and low-temperature phases, we discuss the partial sum rule. It provides information about the effective number of charge carriers for $(tTTF)_2ClO_4$ involved in optical transitions. We calculated the partial sum rule from the optical conductivity spectra polarized along the stacking axis (E || b) at 100 and 293 K according to the following formula [24]:

$$\left[\frac{m_e}{m^*}\right] N_{eff}(\omega) = \frac{m_e}{32\pi N_c e^2} \int_0^{\omega} \sigma_1(\omega')d\omega' , \qquad (2)$$

where m^* is the effective mass of the charge carriers, N_{eff} – effective number of carriers per dimer, N_c – the carrier density (two holes per tTTF tetramer), m_e and e are the mass and electron charge, respectively. The calculations were performed by taking into account the structural data from table 1.

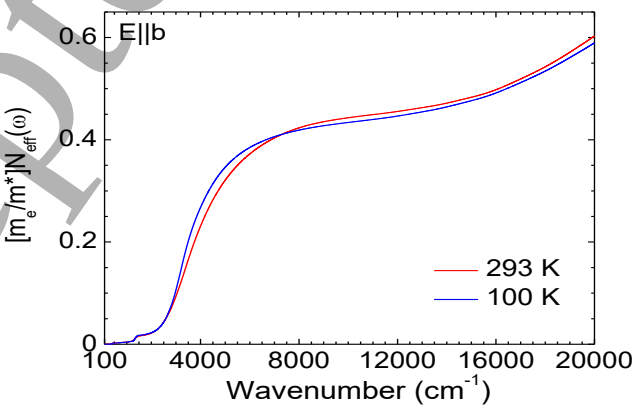

Figure 14. The effective number of charge carriers for $(tTTF)_2ClO_4$ involved in optical transitions, as calculated from the optical conductivity spectra (E || b) for T= 293 and 100 K.

Accepted Manuscript

Figure 14 displays our results, i.e. a plot of the oscillator strength sum rule along the stacking direction (E || b) at T= 293 and 100 K. In the low wavenumber range the $(m_e/m^*)N_{eff}$ increases relatively rapidly and it exists a small difference between curves calculated for two temperatures. Then in the range about 6000-14000 cm^{-1} a plateau is well seen. From the plateau values we estimated the effective mass: $m^*(293\ K) = 2.24m_e$ and $m^*(100\ K) = 2.30m_e$. According to our calculation the effective mass increases about 0.06 m_e in the low-temperature phase of the $(tTTF)_2ClO_4$. However, taking into account an ambiguity of the effective mass evaluation from the plateau regime, the difference might be considered as rather negligible.

The evolutions observed in the frequency and normalized intensity of the ClO_4^- ν_α and ν_β bands (cf figure 10 and figure S5) demonstrate that the anion ordering process observed below T = 137 K affects not only the charge distribution within the tTTF tetramers but also the properties of the ClO_4^- anions themselves. This is at first surprising result for a so-called innocent counter-ion; it might find its explanation in the evolution of the surrounding of the anion and particularly the C–H•••O interactions taking place at the organic-inorganic interface. Such weak interactions [53,54] have been shown to play a crucial role in the electronic properties of molecular TTF-based conductors [5, 55, 56, 57]. Albeit weak in essence, they are found here at H•••O distances notably shorter than the sum of van der Waals radii (O: 1.52 Å + H: 1.20 Å = 2.72 Å). Another indication of the strength is also the linearity of the C–H•••O contacts. Structural characteristics of these interactions are collected in table S4. It appears that the shortest (down to 2.29 Å) and most linear contacts are established between the hydrogen atoms linked to the *sp2* carbon atoms of the tTTF core (figure 15a) and three oxygen atoms of the ClO_4^- anions lying approximately in the tTTF planes.

In the RT structure, both molecules A and B, despite slightly different charge ($\rho = 0.5 \pm \delta_1$), make short C–H•••O contacts. On the other hand, below the phase transition, in the 100 K structure, we observe (figure 15b) that among the four crystallographically independent molecules A-D, the most oxidized ones B and C at the center of the tetramer ($\rho = 0.5 + \delta_2$) are the ones, which interact more strongly with the ClO_4^- anion while the less oxidized A and D molecules ($\rho = 0.5 - \delta_2$) make less and/or longer contacts. There is therefore a clear correlation between the enhanced charge ordering with the tetramers and a distinctive setting of C_{sp2}–H•••O interactions at the organic/inorganic interface, which slightly displace the most oxidized molecules toward the ordered anions.

Furthermore, in the 100 K ordered structure (figure 15b), we note that the shortest and most linear interactions (drawn with thick dotted red lines) concern only three out of the four

Accepted Manuscript

oxygen atoms while one O atom of each ClO_4^- anion, namely atom O_4 on Cl_1 and atom O_5 on Cl_2 (figure 15b) points above and below the plane and interacts much more weakly with the tTTF's hydrogen atoms. This observation can be also tentatively correlated with the actual *intramolecular* Cl–O bonds (table S5) which show an unexpected variability, ranging from 1.423(4) to 1.451(4) Å. It is indeed expected that those O atoms with shorter Cl–O bond distances will exhibit a slightly smaller partial charge (covalency).

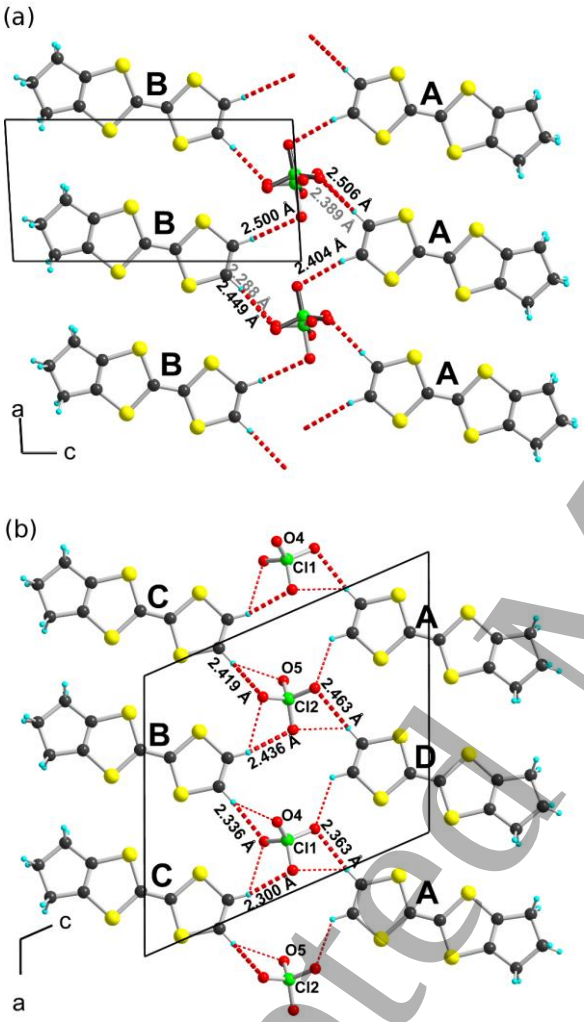

Figure 15. Projection view along the stacking axis of a plane where tTTF molecules and ClO_4^- anions interact through short C–H•••O hydrogen bonds (red dotted lines), (a) at RT, (b) at 100 K.

5. Conclusions

The detailed IR and Raman studies on this tetramerized $(tTTF)_2ClO_4$ salt show that the large charge fluctuations in the high-temperature regime are associated with rather limited

Accepted Manuscript

charge discrepancies between A and B molecules within the BAAB tetramers. However, the charge fluctuations induce short-living charge-rich sites whose average charge density decreases on cooling down. Contrariwise, the charge localization associated with the anion ordering process, which takes place below 137 K, strongly affects the charge distribution within the ABCD tTTF tetramers, with excess charge on the central BC moieties. The charge pattern with …0110… periodicity observed in the $(tTTF)_2ClO_4$ salt below T=137 K is similar to the pattern of other one-dimensional organic conductors with tetramerized stacks. On the other hand, this salt is unique because of the strong fluctuations of delocalized charges above 137 K and the smaller excess of charge on the central BC moieties in tetramers below 137 K.

Band structure calculations performed on the crystal structures, both above and below the transition, show an increase of the semiconducting gap, in accordance with the resistivity increase reported earlier. Determination of the effective number of charge carriers through the partial sum rule confirms that the effective mass increases about 0.06 m_e in the low-temperature phase. A direct link between the charge ordering and the anion ordering processes can be identified from the distinctive setting of C_{sp2}–H•••O interactions at the organic/inorganic interface, up to a point where the Cl–O intramolecular bond lengths within the ClO_4^- anion itself are disymmetrized.

Acknowledgements

We thank for support from German Academic Exchange Service (DAAD). We are also indebted to Jean-Paul Pouget for discussion.

References

[1] Physics of Organic Conductors and Superconductors, ed. A. G. Lebed, Springer Series Vol. 110, Springer-Verlag Berlin Heidelberg (2008)

[2] Aderraba A, Laversanne R, Dupart E, Coulon C, Delhaes P, Hauw C 1983 *J. Phys. Colloq.* **44**, 1243

[3] Fourmigué M, Reinheimer E W, Dunbar K R, Auban-Senzier P, Pasquier C, Coulon C 2008 *Dalton Trans.* **34**, 4652

Accepted Manuscript

[4] Foury-Leylekian P, Auban-Senzier P, Coulon C, Jeannin O, Fourmigué M, Pasquier C and Pouget J-P 2011 *Phys. Rev.* B **84**, 195134

[5] Jeannin O, Reinheimer E W, Foury-Leylekian P, Pouget J-P, Auban-Senzier P, Trzop E, Collet E, Fourmigué M 2018 *IUCrJ* **5**, 361

[6] Delhaes P, Dupart E, Amiell J, Coulon C, Fabre J M, Giral L, Chasseau D, Gallois B 1983 *J. Phys. Colloq.* C3 **44**, 1239

[7] Coulon C, Amiell J, Chasseau D, Manhal E, Fabre J M 1986 *J. Phys. (France)* **47**, 157

[8] Ducasse L, Fritsch A, Chasseau D, Gaultier J 1990 *Synth. Met.* **38**, 13

[9] Ravy S, Foury-Leylekian P, Le Bolloch D, Pouget J-P, Fabre J M, Prado R J, Lagarde P 2004 *J. Phys. IV (France)* **114**, 81

[10] Jankowski D, Świetlik R, Jeannin O, Assaf A, Reinheimer E W, Fourmigué M 2013 *J. Raman Spectr.* **44**, 1765

[11] Łapiński A, Jankowski D, Świetlik R, Reinheimer E W, Fourmigué M 2014 *Synth. Met.* **188**, 92

[12] Heuzé K, Fourmigué M, Batail P, Coulon C, Clérac R, Canadell E, Auban-Senzier P, Ravy S, and Jérome D 2003 *Adv. Mater.* **15**, 1251

[13] Auban-Senzier P, Pasquier C R, Jérome D, Suh S, Brown S E, Mézière C, Batail P 2009 *Phys. Rev. Lett.* **102**, 257001

[14] Zorina L, Simonov S, Mézière C, Canadell E, Suh S, Brown S E, Foury- Leylekian P, Fertey P, Pouget J-P, and Batail P 2009 *J. Mater. Chem.* **19**, 6980

[15] Náfrádi B, Olariu A, Forró L, Mézière C, Batail P, and Jánossy A 2010 *Phys. Rev.* B **81**, 224438

[16] Chasseau D, Gaultier J, Miane J L, Coulon C, Delhaes P, Flandrois S, Fabre J M, Giral L 1983 *J. Phys. Colloq. (France)* **44**, C3-1223

[17] Vaca P, Coulon C, Ravy S, Pouget J-P, Fabre J M 1991 *J. Phys. I (France)* **1**, 125

[18] Fourmigué M, Reinheimer E W, Assaf A, Jeannin O, Saad A, Auban-Senzier P, Alemany P, Rodríguez-Fortea A, Canadell E 2011 *Inorg. Chem.* **50**, 4171

[19] Fabre J-M, Toreilles E, Gibert J P, Chanaa M, Giral L 1977 *Tetrahedron Lett.* **46**, 4033

[20] Fabre J-M, Galaine C, Giral L 1983 *J. Phys. Coll.* **1983**, 1153

[21] Altomare A, Cascarano G, Giacovazzo C, Guagliardi A, Burla M C, G. Polidori G, Camalli M 1994 *J. Appl. Cryst.* **27**, 435

[22] Sheldrick G M 2015 *Acta Cryst.* C **71**, 3

[23] Farrugia L J 2012 *J. Appl. Cryst.* **45**, 849

[24] Wooten F, *Optical Properties of Solids,* 1st ed., Academic Press: NY, USA (1972).

Accepted Manuscript

[25] The Voigt spectroscopy function is a four parameter theoretical model of the spectral line including the Lorentzian and Gaussian types of broadening.

[26] Whangbo M-H and Hoffmann R 1978 *J. Am. Chem. Soc.* **100**, 6093

[27] Ren J, Liang W and Whangbo M-H, *Crystal and Electronic Structure Analysis Using CAESAR*, PrimeColor Software Inc., Cary (NC) USA, 1998

[28] Ammeter J, Bürgi H-B, Thibeault J and Hoffmann R 1978 *J. Am. Chem. Soc.* **100**, 3686

[29] Domercq B, Devic T, Fourmigué M, Auban-Senzier P and Canadell E 2001 *J. Mater. Chem.* **11**, 1570

[30] Gaussian 03 (Revision B.03), M. J. Frisch, G. W. Trucks, H. B. Schlegel, G. E. Scuseria, M. A. Robb, J. R. Cheeseman, J. A. Montgomery, Jr.,T. Vreven, K. N. Kudin, J. C. Burant, J. M. Millam, S. S. Iyengar, J. Tomasi, V. Barone, B. Mennucci, M. Cossi, G. Scalmani, N. Rega, G. A. Petersson, H. Nakatsuji, M. Hada, M. Ehara, K. Toyota, R. Fukuda, J. Hasegawa, M. Ishida, T. Nakajima, Y. Hona, O. Kitao, H. Nakai, M. Klene, X. Li, J. E. Knox, H. P. Hratchian, J. B. Cross, C. Adamo, J. Jaramillo, R. Gomperts, R. E. Stratmann, O. Yazyev, A. J. Austin, R. Cammi, C. Pomelli, J. W. Ochterski, P. Y. Ayala, K. Morokuma, G. A. Voth, P. Salvador, J. J. Dannenberg, V. G. Zakrzewski, S. Dapprich, A. D. Daniels, M. C. Strain, O. Farkas, D. K. Malick, A. D. Rabuck, K. Raghavachari, J. B. Foresman, J. V. Ortiz, Q. Cui, A. G. Baboul, S. Clifford, J. Cioslowski, B. B. Stefanov, G. Liu, A. Liashenko, P. Piskorz, I. Komaromi, R. L. Martin, D. J. Fox, T. Keith, M. A. Al-Laham, C. Y. Peng, A. Nanayakkara, M. Challacombe, P. M. W. Gill, B. Johnson, W. Chen, M. W. Wong, C. Gonzalez, and J. A. Pople, Gaussian, Inc., Pittsburgh PA (2003).

[31] Sun R, Yao J, Li S, Gu R 2008 *Vib. Spectrosc.* **47**, 38

[32] Scott A P, Random L 1996 *J. Phys. Chem.* **100**, 16502

[33] Chasseau D, Gaultier J, Hauw C, Fabre J-M, Giral L, Torreilles E 1978 *Acta Cryst.* B **34**, 2811

[34] Yartsev V M, Graja A 1990 *J. Phys.: Condens. Matt.* **2**, 9631

[35] Dressel M, Drichko N 2004 *Chem. Rev.* **104**, 5689

[36] Łapiński A, Jankowski D, Świetlik R, Reinheimer E W, Fourmigué M 2014 *Synth. Met.* **188**, 92

[37] Pustogow A, Peterseim T, Kolatschek S, Engel L, Dressel M 2016 *Phys. Rev.* B **94**, 195125

[38] Yamamoto T, Uruichi M, Yamamoto K, Yakushi K, Kawamoto A, Taniguchi H 2005 *J. Phys. Chem.* B **109**, 15226

[39] Świetlik R, Barszcz B, Pustogow A, Dressel M 2017 *Phys. Rev.* B **95**, 085205

Accepted Manuscript

[40] Sedlmeier K, Elsässer S, Neubauer D, Beyer R, Wu D, Ivek T, Tomić S, Schlueter J A, Dressel M 2012 *Phys. Rev.* B **86**, 2451031

[41] Shin K-S, Jeannin O, Brezgunova M, Dahaoui S, Aubert E, Espinosa E, Auban-Senzier P, Świetlik R, Frąckowiak A, Fourmigué M 2014 *Dalton Trans.* **43**, 5280

[42] Yamamoto K and Yakushi K 2004 *J. Phys. IV (France)* **114**, 153

[43] Filhol A J and Thomas M 1984 *Acta Cryst.* B **40**, 44

[44] Konno M and Saito Y 1973 *Acta Cryst.* B **29**, 2815

[45] Rindorf G, Thorup N 1988 *Synth. Met.* **25**, 189

[46] Firlej L, Pawlak M, Graja A, Rajchel A, Rizkallah P J, Wallwork S C, and Willis M R 1986 *Acta Phys. Pol*. A **70**, 565

[47] Firlej L, Graja A, Rajchel A, Woźniak K, and Krygowski T M 1987 *Phys. Stat. Sol.* B **140**, 437

[48] Olejniczak I, Graja A 1993 *Acta Phys. Pol.* A **83**, 517

[49] Železný V, Musfeldt J L, Tanner D B 1996 *Adv. Mater. Opt. Electron.* **6**, 353

[50] Świetlik R and Graja A 1983 *J. Phys. (Paris)* **44**, 617

[51] Musfeldt J, Kamaras K, Tanner D B 1992 *Phys. Rev.* B **45**, 10197

[52] Świetlik R 1995 *Synth. Met.* **74**, 115

[53] Desiraju G R, Steiner T, *The Weak Hydrogen Bond*, Oxford University Press, Oxford, (1991).

[54] Aakeröy C B, Evans T A, Seddon K R and Palinko I 1999 *New J. Chem.* **23**, 145

[55] Fourmigué M and Batail P 2004, *Chem. Rev.* **104**, 5379

[56] Whango M-H, Williams J M, Schultz A J, Emge T J and Beno M A 1987 *J. Am. Chem. Soc.* **109**, 90

[57] Dautel O J, Fourmigué M and Canadell E 2001 *Chem.–Eur. J.* **7**, 2635

Accepted Manuscript

Accepted Manuscript